Numerical interaction of boundary waves with perfectly matched layers in elastic waveguides

Kenneth Duru [*], Gunilla Kreiss [†]

April 10, 2012

Abstract

Perfectly matched layers (PML) are a novel technique to simulate the absorption of waves in open domains. Wave propagation in isotropic elastic waveguides has the possibility to support propagating modes with negative group velocities and long wavelengths. Propagating modes with negative group velocities can lead to temporally growing solutions in the PML. In this paper, we demonstrate that negative group velocities in isotropic elastic waveguides are not harmful to the discrete PML. Analysis and numerical experiments confirm the accuracy and the stability of the PML.

Keywords: elastic waves, guided waves, surface waves, perfectly matched layer, group velocity, high order accuracy, stability, SBP-SAT.

1 Introduction

The study of wave propagation in guided structures is important in many engineering applications. For instance, industrial materials such as steel plates and pipes, and natural structures like the earth's surface, can support propagating waves that can lead to failure or disaster. Both theoretical and experimental investigations of wave propagations in guided structures can provide valuable information which can be useful in developing modern technologies or understanding natural disasters such as earthquakes and

[*]Division of Scientific Computing, Department of Information Technology, Uppsala University Sweden

[†]Division of Scientific Computing, Department of Information Technology, Uppsala University Sweden

tsunamis. Numerical simulations can serve as a complement to both theoretical and experimental investigations, and can possibly treat many more important scenarios that can not be accessed theoretically or experimentally. Wave propagation problems are often formulated on infinite or very large spatial domains. In order to perform numerical simulations, large spatial domains must be replaced by smaller computational domains, thereby introducing artificial boundaries. To ensure the accuracy of numerical simulations, artificial boundary conditions must be imposed such that all out–going waves disappear without reflection.

The perfectly matched layer (PML) [38, 2, 22, 33, 35] is an effective method to simulate the absorption of waves in numerical wave simulators. For time-dependent problems, it is important that the PML ensures that all solutions remain bounded for all times. A useful but negative stability result was established in [9]. For hyperbolic systems, it was found that if backward propagating modes (modes with group velocity and the phase velocity of opposite signs) are supported, the corresponding PML will support temporally growing solutions, at sufficiently high frequencies. This undesirable behavior of the PML is largely found in many anisotropic wave equations. For isotropic elastic wave equations, the corresponding Cauchy PML is always stable. However, boundary conditions can introduce many more difficulties. For instance in isotropic elastic waveguides, not only that backward propagating modes can be supported [10]. In the discrete setting, if the boundary conditions are not well treated, the PML can pollute the numerical solutions everywhere [10, 34].

In [18], we considered the PML in a waveguide governed by the time-dependent scalar wave equation. For a waveguide bounded by Neumann boundary conditions, to ensure the accuracy and the stability of the discrete PML, we derived a set of equivalent transformed boundary conditions. The stability of the perfectly matched layer, in the frequency domain, for isotropic elastic waveguides bounded by free–surface boundary condition was considered in [10]. In a recent work [20], we considered a corresponding half–plane problem in the time domain. We derived a PML, together with two mathematically equivalent transformed boundary conditions in the PML. Stability was shown using a mode analysis.

In this paper, we consider the PML in a time–dependent isotropic elastic waveguide. The waveguide is bounded in the y–direction by free–surface boundary conditions, but extends infinitely in the x–direction. Our first objective is to extend the analysis of the half–plane problem to a rectangular waveguide bounded on the top and the bottom by free–surface boundary conditions. We show that if the waveguide supports backward propagating modes, the continuous PML can support temporally growing solutions.

Note that the frequency bands where backward propagating modes exist are rather small and most prominent at lower spatial frequencies [10, 11]. In experiments, experimentalists often use frequencies that do not excite them. This is also useful in computations. In the discrete setting only certain discrete spatial frequencies can be represented. For a finite width PML, numerical approximations can immediately exclude backward propagating modes in the PML.

The second objective of this paper is to numerically evaluate the transformed boundary conditions proposed in [20]. We will use summation–by–parts (SBP) operators [6, 7]. The transformed boundary conditions are imposed weakly using the simultaneous approximation term (SAT) method [3]. An SBP–SAT approximation of the PML for the two equivalent boundary conditions yield two different discrete system of equations. While the first boundary condition yields numerically stable solutions, the second boundary condition supports numerically growing solutions.

The remainder of the paper will proceed as follows. In the next section, we introduce the elastic wave equations and present the well–known results of time–harmonic wave propagation in elastic waveguides. The PML and the corresponding transformed boundary conditions are presented in Section 3. In Section 4, we present the stability analysis. Numerical approximations and discrete stability analysis are presented in Section 5. In Section 6 we perform numerical experiments. In the last section we draw conclusions.

2 Linear elastodynamics

Consider the elastic wave equation for a homogeneous isotropic elastic media in two space dimensions

$$\rho \frac{\partial^2 \mathbf{u}}{\partial t^2} = \nabla \cdot \mathcal{T}, \quad \mathbf{x} \in \Omega, \quad t > 0. \tag{1}$$

Here $\mathbf{x} = (x, y)$ are the spatial variables, t denotes time, Ω is the infinite strip $(x, y) \in (-\infty, \infty) \times (-h, h)$ and ρ is the density of the media. The unknown

$$\mathbf{u} = (u, v)^T,$$

is the displacement vector and $\mathcal{T}$ is the stress tensor. The x and y components of the stress tensor $\mathcal{T}$ are

$$\mathcal{T}_x = A\frac{\partial \mathbf{u}}{\partial x} + C\frac{\partial \mathbf{u}}{\partial y}, \quad \mathcal{T}_y = B\frac{\partial \mathbf{u}}{\partial y} + C^T\frac{\partial \mathbf{u}}{\partial x}.$$

The matrices A, B, C are given by the elastic coefficients. If time is scaled by the density, the system (1) can be rewritten as

$$\frac{\partial^2 \mathbf{u}}{\partial t^2} = \frac{\partial}{\partial x}\left(A\frac{\partial \mathbf{u}}{\partial x}\right) + \frac{\partial}{\partial y}\left(B\frac{\partial \mathbf{u}}{\partial y}\right) + \frac{\partial}{\partial x}\left(C\frac{\partial \mathbf{u}}{\partial y}\right) + \frac{\partial}{\partial y}\left(C^T\frac{\partial \mathbf{u}}{\partial x}\right). \quad (2)$$

The coefficient matrices in (2) are

$$A = \begin{pmatrix} 2\mu+\lambda & 0 \\ 0 & \mu \end{pmatrix}, \quad B = \begin{pmatrix} \mu & 0 \\ 0 & 2\mu+\lambda \end{pmatrix}, \quad C = \begin{pmatrix} 0 & \lambda \\ \mu & 0 \end{pmatrix}, \quad (3)$$

where λ, μ, are the first and second Lamé parameters. The elastic wave equation (2) supports two families of waves, the P–wave and the S–wave with the wave–speeds

$$c_p = \sqrt{2\mu+\lambda}, \quad c_s = \sqrt{\mu},$$

respectively.

2.1 Waveguide

The theory of time–harmonic linear wave propagation in uniform isotropic elastic waveguides is rather well–understood and can be found in many textbooks, see for instance [39]. The foundation was laid by Rayleigh [40] and Lamb [41] about a century ago. A known result is that uniform waveguides of finite thickness allow separable solutions in terms of modes. Secondly propagating waves in elastic waveguides are dispersive, that is waves of different frequencies (or wave numbers) propagate at different phase–speeds. Here we will briefly review these well–known results. More elaborate discussions can be found in [39].

Consider the elastic wave equation (2) in a two dimensional and infinitely long rectangular waveguide of width $L_y = 2h > 0$. On the walls of the waveguide, at $y = \pm h$, we impose the free–surface boundary condition,

$$\mathcal{T}_y := B\frac{\partial \mathbf{u}}{\partial y} + C^T\frac{\partial \mathbf{u}}{\partial x} = 0, \qquad y = \pm h. \quad (4)$$

Let the elastic energy be defined by

$$\mathrm{E}_u(t) := \left\| \frac{\partial \mathbf{u}}{\partial t} \right\|^2 + \int_\Omega \begin{pmatrix} \frac{\partial \mathbf{u}}{\partial x} \\ \frac{\partial \mathbf{u}}{\partial y} \end{pmatrix}^T P \begin{pmatrix} \frac{\partial \mathbf{u}}{\partial x} \\ \frac{\partial \mathbf{u}}{\partial y} \end{pmatrix} d\mathbf{x}, \quad (5)$$

where P is a 4×4 potential energy matrix

$$P = \begin{pmatrix} A & C \\ C^T & B \end{pmatrix}. \quad (6)$$

Note that the elastic wave equation (2) with the free–surface boundary conditions (4) and periodic boundary conditions in the x–direction satisfy

$$\mathrm{E}_u\left(t\right) = \mathrm{E}_u\left(0\right), \quad \forall t > 0. \tag{7}$$

The elastic energy (5) is conserved [19]. Thus the problem (2) with (4) is well–posed.

2.2 Dispersion relation

Assuming that the wave propagates in the x-direction, the wave field takes the form

$$\mathbf{u} = \hat{\mathbf{u}}(y)e^{ik_x x - i\omega t}, \tag{8}$$

where k_x is the spatial wave number and ω is the temporal frequency. Inserting (8) in (2) and (4) we have

$$-\omega^2\hat{\mathbf{u}} = -k_x^2 A\hat{\mathbf{u}} + B\frac{d\hat{\mathbf{u}}}{dy^2} + ik_x\left(C + C^T\right)\frac{d\hat{\mathbf{u}}}{dy}, \tag{9}$$

with the boundary condition

$$B\frac{d\hat{\mathbf{u}}}{dy} + ik_x C^T\hat{\mathbf{u}} = 0, \qquad y = \pm h. \tag{10}$$

The solutions of the ordinary differential equations (9) can be separated [39] into

- symmetric modes

$$\begin{aligned} \hat{u} &= ik_x A_2\cos\left(\kappa_1 y\right) + \kappa_2 B_1\cos\left(\kappa_2 y\right), \\ \hat{v} &= -\kappa_1 A_2\sin\left(\kappa_1 y\right) - ik_x B_1\sin\left(\kappa_2 y\right), \end{aligned} \tag{11}$$

- antisymmetric modes

$$\begin{aligned} \hat{u} &= ik_x A_1\sin\left(\kappa_1 y\right) - \kappa_2 B_2\sin\left(\kappa_2 y\right), \\ \hat{v} &= \kappa_1 A_1\sin\left(\kappa_1 y\right) - ik_x B_2\cos\left(\kappa_2 y\right), \end{aligned} \tag{12}$$

where κ_1, κ_2 are given by

$$\kappa_1 = \sqrt{\frac{\omega^2}{c_p^2} - k_x^2}, \quad \kappa_2 = \sqrt{\frac{\omega^2}{c_s^2} - k_x^2}.$$

Here A_1, A_2, B_1, B_2 are constants to be determined by the boundary conditions. By inserting the solutions (11) and (12) in the boundary condition (10) we obtain the well–known Rayleigh–Lamb dispersion relation, which can be found in many textbooks (see for example [39, 41]),

- symmetric modes

$$F_s(\omega, k_x) \equiv \frac{\tan\left(\sqrt{\hat{\omega}^2 - \hat{k}_x^2}\right)}{\tan\left(\sqrt{\gamma^2\hat{\omega}^2 - \hat{k}_x^2}\right)} + \frac{4\hat{k}_x^2\sqrt{\gamma^2\hat{\omega}^2 - \hat{k}_x^2}\sqrt{\hat{\omega}^2 - \hat{k}_x^2}}{\left(\hat{\omega}^2 - 2\hat{k}_x^2\right)^2} = 0, \tag{13}$$

- antisymmetric modes

$$F_a(\omega, k_x) \equiv \frac{\tan\left(\sqrt{\hat{\omega}^2 - \hat{k}_x^2}\right)}{\tan\left(\sqrt{\gamma^2\hat{\omega}^2 - \hat{k}_x^2}\right)} + \frac{\left(\hat{\omega}^2 - 2\hat{k}_x^2\right)^2}{4\hat{k}_x^2\sqrt{\gamma^2\hat{\omega}^2 - \hat{k}_x^2}\sqrt{\hat{\omega}^2 - \hat{k}_x^2}} = 0. \tag{14}$$

Here

$$\hat{\omega} = \frac{h\omega}{c_s}, \quad \hat{k}_x = k_x h, \quad \gamma = \frac{c_s}{c_p}.$$

The dispersion relations (13) and (14) are non–trivial relationships. However using numerical methods the dispersion curves can be plotted. In figure 1, we have plotted in Matlab the zero contours of the symmetric Rayleigh–Lamb dispersion relation (13) for an aluminum waveguide with $\gamma = 0.4593$. In [10], a root finding software was used to plot the dispersion curves similar to figure 1.

Note that at sufficiently high frequencies $|k_x| \to \infty$ (see [41]), both (13) and (14) yield

$$F_r(\omega, k_x) \equiv \left(\hat{\omega}^2 - 2\hat{k}_x^2\right)^2 + 4\hat{k}_x^2\sqrt{\gamma^2\hat{\omega}^2 - \hat{k}_x^2}\sqrt{\hat{\omega}^2 - \hat{k}_x^2} = 0. \tag{15}$$

It is easily recognized that $F_r(\omega, k_x)$, defined in (15), is the dispersion relation of 'Rayleigh' waves on the surface of an elastic solid, [39, 40, 41].

Since the elastic energy (5) is conserved all roots ω of (13) and (14) are purely real for all $k_x \in \mathbb{R}$. Otherwise, if $\Im\omega \neq 0$, the elastic energy (5) will grow or decay. We introduce the phase velocity v_p and the group velocity v_g which is the velocity of energy propagation, defined by

$$v_p = \frac{\omega}{k_x}, \quad v_g = \frac{d\omega}{dk_x}.$$

Implicit differentiation yields

$$v_g = -\left(\frac{\partial F_j}{\partial \omega}\right)^{-1}\frac{\partial F_j}{\partial k_x}, \quad j = s, a.$$

From the plot of the dispersion relations (13) and (14) see figure (1), the phase velocity v_p and the group velocity v_g can be easily obtained.

Note that when $\omega > 0$ and $k_x > 0$ the phase velocity is positive $v_p > 0$. This is not always the case for the group velocity. The group velocity can be negative when the phase velocity is positive. This implies that information propagates in one direction while energy propagates in the opposite direction. When the phase velocity and the group velocity have opposite signs the corresponding mode is called a backward propagating mode. Backward propagating modes can cause unwanted growth in the PML.

In figure 1, the second symmetric mode has oppositely directed group and phase velocities at very long wavelengths $0 < \hat{k}_x < 1$.

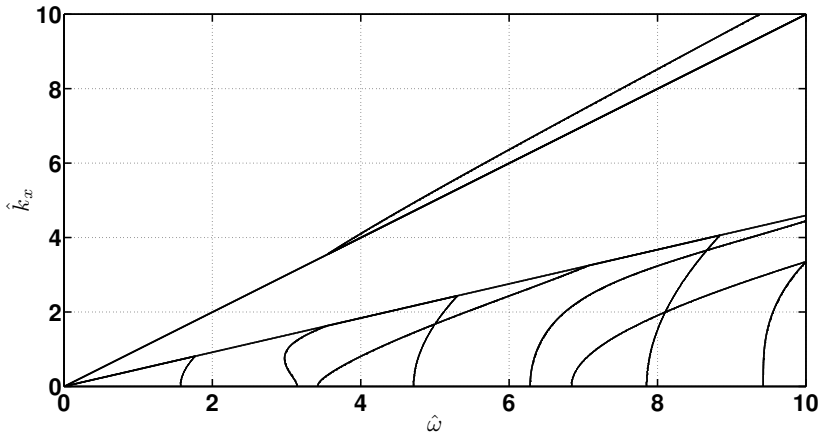

Figure 1: *Zero contours of the symmetric Rayleigh–Lamb dispersion relation (13).*

3 The perfectly matched layer

Assume that we want to compute the solution of the elastic wave equation (2) in the rectangular waveguide $-L_x \leq x \leq L_x$, $-h < y < h$ and the PML is introduced outside the domain, that is, in $|x| > L_x, -h < y < h$. At the walls $y = \pm h$, the free–surface boundary condition (4) is imposed. The

PML we will use in this paper was derived in [20]. The PML equation reads

$$\begin{aligned}
\frac{\partial^2 \mathbf{u}}{\partial t^2} + \sigma \frac{\partial \mathbf{u}}{\partial t} =& \frac{\partial}{\partial x}\left(A\frac{\partial \mathbf{u}}{\partial x} + C\frac{\partial \mathbf{u}}{\partial y}\right) + \frac{\partial}{\partial y}\left(B\frac{\partial \mathbf{u}}{\partial y} + C^T\frac{\partial \mathbf{u}}{\partial x}\right) \\
& - A\frac{\partial(\sigma \mathbf{v})}{\partial x} + B\frac{\partial(\sigma \mathbf{w})}{\partial y} + \sigma\alpha\left(\mathbf{u} - \mathbf{q}\right), \\
\frac{\partial \mathbf{v}}{\partial t} =& -\left(\sigma + \alpha\right)\mathbf{v} + \frac{\partial \mathbf{u}}{\partial x}, \\
\frac{\partial \mathbf{w}}{\partial t} =& -\alpha \mathbf{w} + \frac{\partial \mathbf{u}}{\partial y}, \\
\frac{\partial \mathbf{q}}{\partial t} =& \alpha\left(\mathbf{u} - \mathbf{q}\right),
\end{aligned} \tag{16}$$

and corresponding transformed boundary conditions are

$$B\frac{\partial \mathbf{u}}{\partial y} + C^T\frac{\partial \mathbf{u}}{\partial x} + \sigma B\mathbf{w} = 0, \quad y = \pm h, \tag{17}$$

or

$$B\frac{\partial \mathbf{u}}{\partial y} + C^T\frac{\partial \mathbf{u}}{\partial x} - \sigma C^T\mathbf{v} = 0, \quad y = \pm h. \tag{18}$$

Here, $\sigma(x) \geq 0$ is the damping function and $\alpha \geq 0$ is the complex frequency shift. Note that the boundary conditions (17) and (18) are mathematically equivalent, see [20]. We also note in passing that when the damping vanishes $\sigma \equiv 0$, we recover completely the wave equation (2) and the free–surface boundary condition (4). It is possible to impose the free–surface boundary condition (4), without modification. However, using (4) only as a boundary condition is not consistent with the PML and can lead to exponentially growing solutions in the PML.

In the absence of boundaries, the PML model (16) is perfectly matched to the elastic wave equation (2) if $\sigma(\pm L_x) = 0$. There are no reflections as waves pass the interfaces at $x = \pm L_x$. That is, waves of all frequencies and angles are transmitted from the interior into the layer without any reflections. Secondly, the PML damps waves so that they become insignificant before they reach the outer boundary of the computational domain. We initialize the fields in the PML with homogeneous initial data

$$\mathbf{u}(x, y, 0) = 0, \quad \frac{\partial \mathbf{u}}{\partial t}(x, y, 0) = 0,$$

$$\mathbf{v}(x, y, 0) = 0, \quad \mathbf{w}(x, y, 0) = 0, \quad \mathbf{q}(x, y, 0) = 0.$$

4 Stability analysis of the PML

In this section, our goal is to extend the stability analysis [9] for the Cauchy problem, and the stability analysis [20] for the corresponding half plane

problem, to a uniform isotropic elastic waveguide bounded by free–surface boundary conditions. We will show that in a uniform isotropic elastic waveguide, if there are backward propagating modes, for sufficiently small constant damping, the PML can support temporally growing solutions. However, at sufficiently high frequencies we regain the Rayleigh dispersion relation (15). Any $\sigma \geq 0$ will move all modes into the stable half complex pane. Thus showing the stability of the PML at sufficiently high frequencies.

4.1 Continuous analysis

As before we make the ansatz,

$$\mathbf{V} = \hat{\mathbf{V}}(y)e^{ik_x x - i\omega t}, \quad |\hat{\mathbf{V}}(y)| < \infty. \tag{19}$$

Inserting (19) in (16), and (17) or (18) yields the boundary value problem

$$-\omega^2 \hat{\mathbf{u}} = -\tilde{k}_x^2 A\hat{\mathbf{u}} + B\frac{d^2\hat{\mathbf{u}}}{dy^2} + i\tilde{k}_x\left(C + C^T\right)\frac{d\hat{\mathbf{u}}}{dy}, \tag{20}$$

$$B\frac{d\hat{\mathbf{u}}(i\tilde{k}_x, y, s)}{dy} + i\tilde{k}_x C^T \hat{\mathbf{u}}(i\tilde{k}_x, y, s) = 0, \quad y = \pm h, \tag{21}$$

where

$$\tilde{k}_x = \frac{k_x}{S_x}, \quad S_x = 1 + \frac{\sigma}{\alpha + i\omega}.$$

The introduction of the transformed spatial wave number $\tilde{k}_x$ simplifies the remaining part of the analysis. Note the similarity between (20), (21) and the boundary value problem (9), (10). As before, considering the symmetric and the anti–symmetric modes separately we obtain the corresponding dispersion relation

- symmetric modes

$$F_s\left(\omega, \hat{\tilde{k}}_x\right) \equiv \frac{\tan\left(\sqrt{\hat{\omega}^2 - \hat{\tilde{k}}_x^2}\right)}{\tan\left(\sqrt{\gamma^2\hat{\omega}^2 - \hat{\tilde{k}}_x^2}\right)} + \frac{4\hat{\tilde{k}}_x^2\sqrt{\gamma^2\hat{\omega}^2 - \hat{\tilde{k}}_x^2}\sqrt{\hat{\omega}^2 - \hat{\tilde{k}}_x^2}}{\left(\hat{\omega}^2 - 2\hat{\tilde{k}}_x^2\right)^2} = 0, \tag{22}$$

- antisymmetric modes

$$F_a\left(\omega, \hat{\tilde{k}}_x\right) \equiv \frac{\tan\left(\sqrt{\hat{\omega}^2 - \hat{\tilde{k}}_x^2}\right)}{\tan\left(\sqrt{\gamma^2\hat{\omega}^2 - \hat{\tilde{k}}_x^2}\right)} + \frac{\left(\hat{\omega}^2 - 2\hat{\tilde{k}}_x^2\right)^2}{4\hat{\tilde{k}}_x^2\sqrt{\gamma^2\hat{\omega}^2 - \hat{\tilde{k}}_x^2}\sqrt{\hat{\omega}^2 - \hat{\tilde{k}}_x^2}} = 0, \tag{23}$$

where $\hat{\tilde{k}}_x = h\tilde{k}_x$. If there are roots ω of (22) or (23) with $\Im\omega < 0$ we say that the constant coefficient PML (16) with the boundary condition (17) or (18) supports temporally growing solutions.

Proposition 1 *Consider the constant coefficient PML (16) in the infinite strip $\Omega = (-\infty, \infty) \times (-h, h)$ subject to the boundary condition (17) or (18) at $y = \pm h$. Let v_p denote the phase velocity and v_g denote the group velocity. For any bounded k_x, $0 < |k_x| < k_\infty$, and sufficiently small damping $0 < \sigma \ll 1$, backward propagating modes will support temporally growing solutions in the PML.*

Proof:

For any bounded k_x and for sufficiently small damping we write

$$\omega = \omega_0 + \omega_\sigma \sigma,$$

where ω_0 is the purely real root of (13) or (14) (when $\sigma = 0$). Thus growth is determined by the sign of the imaginary part of ω_σ. Consider

$$F_j\left(\omega_0, \hat{k}_x\right) + \sigma \frac{\partial F_j\left(\omega, \hat{\tilde{k}}_x\right)}{\partial \sigma}\Big|_{\sigma=0} = 0, \quad j = s, a.$$

We know that $F_j\left(\omega_0, \hat{k}_x\right) \equiv 0$, therefore

$$\frac{\partial F_j\left(\omega, \hat{\tilde{k}}_x\right)}{\partial \sigma} = \frac{\partial \omega}{\partial \sigma} \frac{\partial F_j\left(\omega, \hat{\tilde{k}}_x\right)}{\partial \omega}\Big|_{\sigma=0} - \frac{k_x}{\alpha + i\omega} \frac{\partial F_j\left(\omega, \hat{\tilde{k}}_x\right)}{\partial k_x}\Big|_{\sigma=0} = 0,$$

and

$$\omega_\sigma \equiv \frac{\partial \omega}{\partial \sigma} = \frac{k_x}{\alpha + i\omega} \left(\frac{\partial F_j\left(\omega, k_x\right)}{\partial \omega}\right)^{-1} \frac{\partial F_j\left(\omega, k_x\right)}{\partial k_x}.$$

We have

$$\Im\omega_\sigma = \frac{|\omega|^2}{|\alpha|^2 + |\omega|^2} \frac{k_x}{\omega} \left(-\frac{\partial F_j\left(\omega, k_x\right)}{\partial \omega}\right)^{-1} \frac{\partial F_j\left(\omega, k_x\right)}{\partial k_x},$$

$$\Im\omega_\sigma = \frac{|\omega|^2}{|\alpha|^2 + |\omega|^2} \frac{v_g v_p}{|v_p|^2}.$$

Therefore, if $v_g v_p < 0$ the PML will support growth, at least for sufficiently small damping $\sigma > 0$. □

At sufficiently high frequencies a more refined analysis is needed.

Proposition 2 *Consider the constant coefficient PML (16) in the infinite strip $\Omega = (-\infty, \infty) \times (-h, h)$ subject to the boundary condition (17) or (18) at $y = \pm h$. At sufficiently high frequencies $|k_x| \to \infty$, the PML is stable.*

Proof:

Introduce the normalized variables

$$\eta = \frac{\omega}{|k_x|}, \quad k_1 = \frac{k_x}{|k_x|} \quad \epsilon = \frac{\sigma}{|k_x|}, \quad \nu = \frac{\alpha}{|k_x|}. \tag{24}$$

At sufficiently high frequencies $|k_x| \to \infty$, the normalized variables (24) satisfy

$$F_r\left(\eta, \frac{i\eta + \nu}{i\eta + \nu + \epsilon} k_1\right) = 0, \tag{25}$$

where $F_r(\omega, k_x)$ is the dispersion relation for Rayleigh waves define in (15). Note that $F_r(\omega, k_x)$ is a homogeneous function of degree four, we have

$$\left(\frac{i\eta + \nu}{i\eta + \nu + \epsilon}\right)^4 F_r\left(\eta \frac{i\eta + \nu + \epsilon}{i\eta + \nu}, k_1\right) = 0. \tag{26}$$

All roots ν of (26) are a multiple root $\eta = i\nu$, or satisfies

$$F_r\left(\eta \frac{i\eta + \nu + \epsilon}{i\eta + \nu}, k_1\right) = 0. \tag{27}$$

Note that

$$\eta \frac{i\eta + \nu + \epsilon}{i\eta + \nu} = \eta_0. \tag{28}$$

Here, η_0 is the purely real root of $F_r(\eta_0, k_1) = 0$. When $\alpha \equiv 0$ we have

$$\eta = 0, \quad \eta = i\epsilon + \eta_0.$$

Note that when $\alpha > 0$, a combination of standard perturbation and continuity arguments show that all roots η of (25) satisfy $\Im\eta \geq 0$ for all $\sigma > 0$ (see [20] for more details). □

In the next subsection we will compute the temporal eigenvalues corresponding the semi–discrete (continuous in x but discrete in y) spatial operator.

4.2 Semi–discrete analysis

We will verify the above continuous analyses and demonstrate the semi–discrete effects of the transformed boundary conditions (17) and (18). By taking Fourier transform in the x–direction and discretizing the y–direction, we have the corresponding eigenvalue problem

$$\left(\mathbf{P}_b - \lambda \mathbf{I}\right) \mathbf{U} = 0, \quad b = 1, 2, \quad \mathbf{U} = \left(\mathbf{u}, \mathbf{u}_t, \mathbf{v}, \mathbf{w}, \mathbf{q}\right)^T. \tag{29}$$

Here $\mathbf{P}_b$ is the semi–discrete spatial operator including the transformed boundary condition (17) when $b = 1$, and (18) when $b = 2$. For the transformed boundary condition (17) the corresponding spatial operator is

$$P_1 = \begin{pmatrix} \mathbf{0} \otimes \mathbf{I} & \mathbf{I}_2 \otimes \mathbf{I} & \mathbf{0} \otimes \mathbf{I} & \mathbf{0} \otimes \mathbf{I} & \mathbf{0} \otimes \mathbf{I} \\ \mathbf{L} + \eta\sigma \left(\mathbf{I}_2 \otimes \mathbf{I}\right) & -\sigma \left(\mathbf{I}_2 \otimes \mathbf{I}\right) & -ik_x \sigma A \otimes \mathbf{I} & \sigma B \otimes \left(D_1 - \tau B_N\right) & -\eta\sigma \left(\mathbf{I}_2 \otimes \mathbf{I}\right) \\ ik_x \mathbf{I}_2 \otimes \mathbf{I} & \mathbf{0} \otimes \mathbf{I} & -\left(\alpha + \sigma\right) \mathbf{I}_2 \otimes \mathbf{I} & \mathbf{0} \otimes \mathbf{I} & \mathbf{0} \otimes \mathbf{I} \\ \mathbf{I}_2 \otimes \mathbf{D_1} & \mathbf{0} \otimes \mathbf{I} & \mathbf{0} \otimes \mathbf{I} & -\alpha \mathbf{I}_2 \otimes \mathbf{I} & \mathbf{0} \otimes \mathbf{I} \\ \alpha \mathbf{I}_2 \otimes \mathbf{I} & \mathbf{0} \otimes \mathbf{I} & \mathbf{0} \otimes \mathbf{I} & \mathbf{0} \otimes \mathbf{I} & -\alpha \mathbf{I}_2 \otimes \mathbf{I} \end{pmatrix},$$

and

$$P_2 = \begin{pmatrix} \mathbf{0} \otimes \mathbf{I} & \mathbf{I}_2 \otimes \mathbf{I} & \mathbf{0} \otimes \mathbf{I} & \mathbf{0} \otimes \mathbf{I} & \mathbf{0} \otimes \mathbf{I} \\ \mathbf{L} + \eta\sigma \left(\mathbf{I}_2 \otimes \mathbf{I}\right) & -\sigma \left(\mathbf{I}_2 \otimes \mathbf{I}\right) & -ik_x \sigma A \otimes \mathbf{I} + \tau\sigma \left(C^T \otimes B_N\right) & \sigma B \otimes \left(D_1\right) & -\eta\sigma \left(\mathbf{I}_2 \otimes \mathbf{I}\right) \\ ik_x \mathbf{I}_2 \otimes \mathbf{I} & \mathbf{0} \otimes \mathbf{I} & -\left(\alpha + \sigma\right) \mathbf{I}_2 \otimes \mathbf{I} & \mathbf{0} \otimes \mathbf{I} & \mathbf{0} \otimes \mathbf{I} \\ \mathbf{I}_2 \otimes \mathbf{D_1} & \mathbf{0} \otimes \mathbf{I} & \mathbf{0} \otimes \mathbf{I} & -\alpha \mathbf{I}_2 \otimes \mathbf{I} & \mathbf{0} \otimes \mathbf{I} \\ \alpha \mathbf{I}_2 \otimes \mathbf{I} & \mathbf{0} \otimes \mathbf{I} & \mathbf{0} \otimes \mathbf{I} & \mathbf{0} \otimes \mathbf{I} & -\alpha \mathbf{I}_2 \otimes \mathbf{I} \end{pmatrix}$$

for the transformed boundary condition (18). Here,

$$\mathbf{L} = -k_x^2 A \otimes \mathbf{I} + ik_x \left(C + C^T\right) \otimes D_1 + B \otimes D_2 - \tau \left(I_2 \otimes H^{-1} B_N\right) \left(B \otimes D_1 + ik_x C^T \otimes I\right),$$

is the spatial operator for the elastic wave equation (2) with a SAT imposition of the free–surface boundary condition (4). The matrices D_1, D_2 are SBP operators (defined in the next section) approximating $\partial/\partial y$ and $\partial^2/\partial y^2$ respectively, H is the corresponding H–norm, $B_N = \text{ diag}(-1, 0, \ldots, 0, 1)$ is a boundary operator, $\tau = 1$ is a penalty term and k_x is the non–dimensional wavenumber. Furthermore, $\mathbf{0}$ is a 2×2 zero matrix, $\mathbf{I}_2$ is a 2×2 identity matrix, $\mathbf{I}$ is a $N \times N$ identity matrix, where N is the number of grid points in the interval $[-1, 1]$.

If there are eigenvalues λ of P_b with $\Re\lambda > 0$, the operator P_b will support solutions with growing amplitude in time.

We set $\sigma = 1, \alpha = 0.1$. Consider the aluminum waveguide defined by the velocity ratio $\gamma = 0.4593$. By Proposition 1, for the aluminum waveguide we know that for sufficiently small damping $\sigma > 0$, some eigenvalues $\lambda\left(k_x, \sigma\right)$ with $0 < k_x < 1$ have positive real parts, $\Re\lambda > 0$. For higher spatial

wavenumbers, by Proposition 2 all eigenvalues $\lambda(k_x, \sigma)$ with $k_x > 1$ have non–positive real parts, $\Re\lambda \leq 0$. To compute the eigenvalues of the operator P_b we consider the spatial wave numbers $k_x = [0 : 0.1 : 10]$, and discretize in the y-direction (the interval $[-1, 1]$) with $N = 101$ grid points.

In figure 2, we have plotted the eigenvalues of of the operators P_1 and P_2, and the maximum real parts of the eigenvalues as a function of the spatial wave number k_x. Note that for the operator P_1 only eigenvalues with $0 < k_x < 1$ have positive real parts. On the other hand the operator P_2 have eigenvalues with positive real parts for $0 < k_x < 5$. The extra eigenvalues with positive real parts are purely real, and correspond to multiple zero eigenvalues when $\sigma \equiv 0$. For the spatial operator P_2, when $\sigma > 0$ some of the multiple zero eigenvalues move into the right half of the complex plane.

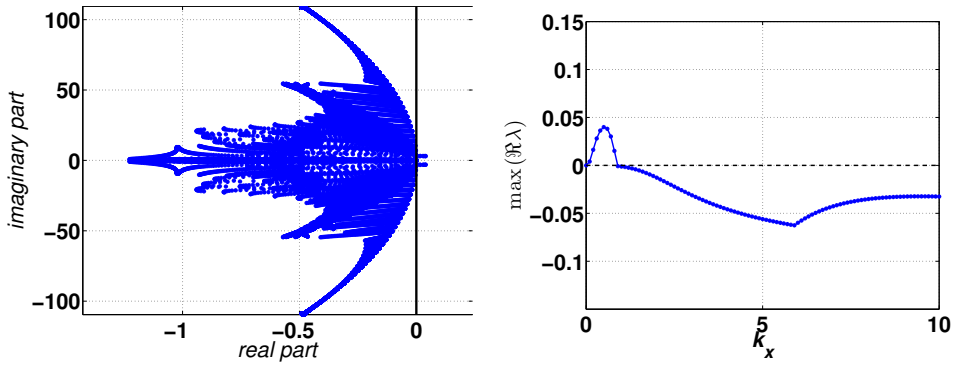

(a) eigenvalues of the operator P_1 with (17). (b) $\max(\Re\lambda)$ as a function of the wavenumber k_x for (17).

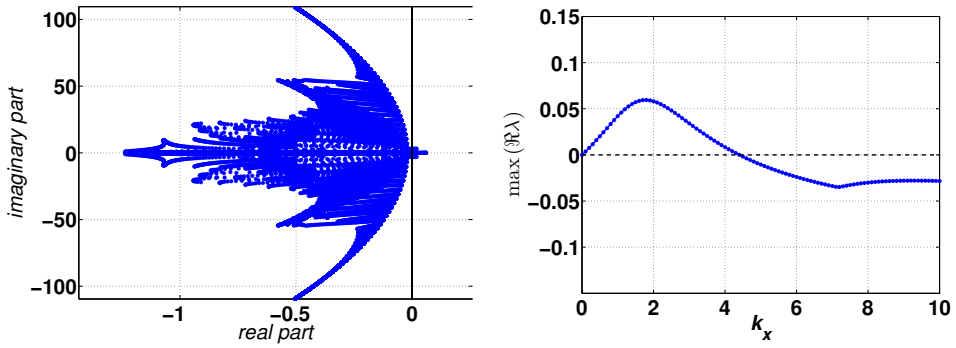

(c) eigenvalues of the operator P_2 with (18). (d) $\max(\Re\lambda)$ as a function of the wavenumber k_x for (18).

Figure 2: *Temporal eigenvalues of the spatial operator P_b. The top panel corresponds to the transformed boundary condition (17) and the lower panel corresponds to the transformed boundary condition (18).*

5 Numerical method

In this section, we derive SBP–SAT approximations for the PML. We will briefly discuss the SBP-SAT framework for second order systems. More elaborate discussion of the numerical method can be found in our recent paper [19]. We will also demonstrate the numerical stability of the transformed boundary conditions (17) and (18).

5.1 Discrete operators

Consider the rectangular computational domain $(x, y) \in [-(x_0 + \delta), x_0 + \delta] \times [-y_0, y_0]$, with $x_0, y_0 > 0$. Here $\delta \geq 0$ is the width of the PML. Let the grid in (x, y) coordinates be defined by

$$x_j = -(x_0 + \delta) + (j-1)\,\Delta x, \quad j = 1, 2, \cdots, N_x - 1, N_x, \quad \Delta x = \frac{2(x_0 + \delta)}{N_x - 1},$$
$$y_i = -y_0 + (i-1)\,\Delta y, \quad i = 1, 2, \cdots, N_y - 1, N_y, \quad \Delta y = \frac{2y_0}{N_y - 1},$$

where $N_x, N_y \in \mathbb{N}$ are the number of grid points used in the x– and the y–directions respectively. The grid function is denoted $[\mathbf{u}_{i,j}]$. Note that we can always rearrange the grid–function $\mathbf{u}_{i,j}$ as a vector $\mathbf{u}$ of length $2N_xN_y$.

Let D_1, D_2 be discrete operators approximating the first and the second derivatives respectively, that is

$$D_1 \approx \frac{\partial}{\partial x}, \quad D_2 \approx \frac{\partial^2}{\partial x^2}.$$

The discrete operators D_1, D_2 are (one dimensional) summation–by–parts (SBP) operators if they satisfy the following properties

$$\begin{aligned} &D_1 = H^{-1}Q, \quad Q^T + Q = B_N, \\ &B_N = \mathrm{diag}(-1, 0, 0, \ldots, 1), \quad H = H^T, \quad \mathbf{v}^T H \mathbf{v} > 0, \end{aligned} \tag{30}$$

$$\begin{aligned} &D_2 = H^{-1}(-M + B_N S), \quad M = M^T, \\ &\mathbf{v}^T M \mathbf{v} \geq 0, \quad H = H^T, \quad \mathbf{v}^T H \mathbf{v} > 0. \end{aligned} \tag{31}$$

Here $\mathbf{v}$ is a vector of length N_x, Q is almost a skew-symmetric operator, M is called the symmetric part of the operator D_2 and the operator S is a one–sided approximation of the first derivative $\partial/\partial x$ on the boundaries. Further, H defines a norm, $\|\mathbf{v}\|_H = \mathbf{v}^T H \mathbf{v}$, which is equivalent to the standard discrete norm $\|\mathbf{v}\| = \Delta x \mathbf{v}^T \mathbf{v}$, when $H = \Delta x I$.

Discrete operators satisfying the summation-by-parts properties (30), (31) are usually derived using 2r–order ($r = 1, 2, \ldots$) standard centered difference schemes away from the boundaries. Close to the boundaries lower

order schemes (usually of order r) are used such that the operators satisfy (30), (31) in a given H–norm. The operator H can be a diagonal norm or a block norm. In this work we will use the diagonal norm SBP operators presented in [6] for $r = 1, 2$. More elaborate discussions of SBP operators can be found in the selected references [7, 5, 6].

The discrete operators in higher space dimensions can be constructed using the Kronecker product defined below.

Definition 1 (Kronecker Products) *Let A be an m-by-n matrix and B be a p-by-q matrix. Then $A \otimes B$, the Kronecker product of A and B, is the (m.p)-by-(n.q) matrix*

$$A \otimes B = \begin{pmatrix} a_{11}B & a_{12}B & \dots & a_{1m}B \\ . & . & . & . \\ . & . & . & . \\ a_{n1}B & a_{n2}B & \dots & a_{nm}B \end{pmatrix}.$$

The following properties hold for Kronecker products

1. Assume that the products A·C and B·D are well defined then $(A \otimes B) \cdot (C \otimes D) = (A \cdot C) \otimes (B \cdot D)$

2. If A and B are invertible, then $(A \otimes B)^{-1} = A^{-1} \otimes B^{-1}$

3. $(A \otimes B)^T = A^T \otimes B^T$

We introduce the two dimensional discrete spatial operators

$$\begin{aligned} &D_x = I_y \otimes D_1, \quad D_y = D_1 \otimes I_x, \quad D_{ny} = S \otimes I, \quad B_{ny} = B_N \otimes I, \quad H_x = I \otimes H, \\ &D_{xx} = I_y \otimes D_2, \quad D_{yy} = D_2 \otimes I_x, \quad D_{xy} = D_{yx} = D_1 \otimes D_1, \quad H_y = H \otimes I. \end{aligned} \tag{32}$$

Here I_x, I_y are identity operators with dimensions N_x and N_y respectively. The operators H_x, H_y are symmetric and positive definite and therefore define discrete norms.

5.2 Semi-discrete approximation

The SBP operators defined in the last subsection will be used to approximate the spatial derivatives. Dirichlet boundary conditions will be imposed strongly, while other boundary conditions will be imposed using SAT.

A semi–discrete approximation of the auxiliary differential equations is

$$\begin{aligned}
\frac{d\mathbf{v}}{dt} &= -\left(\sigma+\alpha\right)\mathbf{v} + \left(I_2 \otimes D_x\right)\mathbf{u}, \\
\frac{d\mathbf{w}}{dt} &= -\alpha\mathbf{w} + \left(I_2 \otimes D_y\right)\mathbf{u}, \\
\frac{d\mathbf{q}}{dt} &= \alpha\left(\mathbf{u}-\mathbf{q}\right).
\end{aligned} \tag{33}$$

At $y = \pm y_0$, we will compare imposing the the transformed boundary conditions (17) and (18). In the x–direction, at $x = \pm\left(x_0+\delta\right)$, we impose homogeneous Dirichlet boundary conditions on the displacement field,

$$\mathbf{u} = 0, \quad x = \pm\left(x_0+\delta\right). \tag{34}$$

We will combine (33) with a SBP–SAT approximation of the transformed wave equation which reads

$$\frac{d^2\mathbf{u}}{dt^2} + \sigma\frac{d\mathbf{u}}{dt} = L\mathbf{u} + F_b\left(\mathbf{u},\mathbf{v},\mathbf{w},\mathbf{q},\sigma,\alpha\right), \quad b = 1, \quad \text{or} \quad b = 2, \tag{35}$$

where

$$\begin{aligned}
L = &\left(A \otimes D_{xx}\right) + \left(C \otimes D_{yx}\right) + \left(B \otimes D_{yy}\right) + \left(C^T \otimes D_{xy}\right) \\
&- \tau\left(I_2 \otimes H_y^{-1}\right)\left(I_2 \otimes B_{ny}\right)\left(B \otimes D_{ny} + C^T \otimes D_x\right),
\end{aligned} \tag{36}$$

is the spatial approximation for the elastic wave equation (2) with a SAT imposition of the free–surface boundary condition (4). The Dirichlet boundary condition (34) is explicitly imposed. The forcing function $F_b\left(\mathbf{u},\mathbf{v},\mathbf{w},\mathbf{q},\sigma,\alpha\right)$ ensures perfect matching. Note that $b = 1$ corresponds to the transformed boundary condition (17) and $b = 2$ corresponds to the transformed boundary condition (18). When $b = 1$ we have

$$\begin{aligned}
F_1\left(\mathbf{u},\mathbf{v},\mathbf{w},\mathbf{q},\sigma,\alpha\right) = &-\left(A \otimes D_x\right)\left(\sigma\mathbf{v}\right) + \left(B \otimes D_y\right)\left(\sigma\mathbf{w}\right) + \sigma\alpha\left(\mathbf{u}-\mathbf{q}\right) \\
&- \tau\sigma\left(I_2 \otimes H_y^{-1}\right)\left(I_2 \otimes B_{ny}\right)\left(B \otimes I\right)\mathbf{w},
\end{aligned} \tag{37}$$

and $b = 2$ yields

$$\begin{aligned}
F_2\left(\mathbf{u},\mathbf{v},\mathbf{w},\mathbf{q},\sigma,\alpha\right) = &-\left(A \otimes D_x\right)\left(\sigma\mathbf{v}\right) + \left(B \otimes D_y\right)\left(\sigma\mathbf{w}\right) + \sigma\alpha\left(\mathbf{u}-\mathbf{q}\right) \\
&+ \tau\sigma\left(I_2 \otimes H_y^{-1}\right)\left(I_2 \otimes B_{ny}\right)\left(C^T \otimes I\right)\mathbf{v}.
\end{aligned} \tag{38}$$

Here $\tau = 1$ is a penalty. Note that when $\sigma \equiv 0$ the semi–discrete approximation (35) satisfies a strict energy estimate, see [19].

5.3 Numerical stability of the PML

In this subsection, we will demonstrate the numerical stability of the SAT boundary treatment for the semi–discrete approximations (33) and (35). Since we are interested in the numerical boundary treatments, we will first consider a corresponding 1D problem and derive continuous and the corresponding discrete energy estimates. For the 2D discrete PML, we will compute the fully discrete temporal eigenvalues corresponding to the spatial discrete operators.

5.3.1 1D problem and energy estimates

Consider the 1D problem with $\partial/\partial x \equiv 0$

$$\begin{aligned}
\frac{\partial^2 \mathbf{u}}{\partial t^2} + \sigma \frac{\partial \mathbf{u}}{\partial t} &= \frac{\partial}{\partial y}\left(B\frac{\partial \mathbf{u}}{\partial y} + \sigma B \mathbf{w} \right) + \sigma\alpha\left(\mathbf{u}-\mathbf{q}\right), \\
\frac{\partial \mathbf{v}}{\partial t} &= -\left(\sigma+\alpha\right)\mathbf{v}, \\
\frac{\partial \mathbf{w}}{\partial t} &= -\alpha\mathbf{w} + \frac{\partial \mathbf{u}}{\partial y}, \\
\frac{\partial \mathbf{q}}{\partial t} &= \alpha\left(\mathbf{u}-\mathbf{q}\right),
\end{aligned} \tag{39}$$

and the corresponding transformed boundary conditions

$$B\frac{\partial \mathbf{u}}{\partial y} + \sigma B \mathbf{w} = 0, \quad y = \pm y_0, \tag{40}$$

or

$$B\frac{\partial \mathbf{u}}{\partial y} - \sigma C^T \mathbf{v} = 0, \quad y = \pm y_0. \tag{41}$$

Note that a corresponding scalar problem to (39) has been recently studied in [18]. To derive an estimate we first introduce the relevant energy norm

$$\begin{aligned}
E_\sigma(t) = &\int_{-y_0}^{y_0} \left(\frac{\partial \mathbf{u}}{\partial t}^T \frac{\partial \mathbf{u}}{\partial t} + \left(\frac{\partial \mathbf{u}}{\partial y} + \sigma\mathbf{w} \right)^T B \left(\frac{\partial \mathbf{u}}{\partial y} + \sigma\mathbf{w} \right) \right) dy \\
&+ \int_{-y_0}^{y_0} \left(\left(\sigma\mathbf{w}\right)^T B\left(\sigma\mathbf{w}\right) + \left(\mathbf{u}-\mathbf{q}\right)^T \alpha\sigma\left(\mathbf{u}-\mathbf{q}\right) \right) dy.
\end{aligned} \tag{42}$$

Note that when $\sigma \equiv 0$ we get the standard physical energy for the wave equation

$$E(t) = \int_{-y_0}^{y_0} \left(\frac{\partial \mathbf{u}}{\partial t}^T \frac{\partial \mathbf{u}}{\partial t} + \frac{\partial \mathbf{u}}{\partial y}^T B \frac{\partial \mathbf{u}}{\partial y} \right) dy. \tag{43}$$

Proposition 3 *The 1D perfectly matched layer (39) subject to the transformed boundary conditions (40) and (41) at $y = \pm y_0$ satisfies the energy estimate*

$$\sqrt{E_\sigma(t)} \leq e^{\beta t}\sqrt{E_\sigma(0)}, \quad \beta = \alpha_\infty + \sigma_\infty. \tag{44}$$

Proof:

To derive the estimate (44), we multiply the first equation in (39) by $(\partial \mathbf{u}/\partial t)^T$ and integrate over $y \in [-y_0, y_0]$. Integration by parts yields

$$\begin{aligned}
&\int_{-y_0}^{y_0} \frac{\partial \mathbf{u}}{\partial t}^T \frac{\partial^2 \mathbf{u}}{\partial t^2} dy + \int_{-y_0}^{y_0} \frac{\partial \mathbf{u}}{\partial t}^T \sigma \frac{\partial \mathbf{u}}{\partial t} dy - \int_{-y_0}^{y_0} \frac{\partial \mathbf{u}}{\partial t}^T \sigma\alpha\,(\mathbf{u}-\mathbf{q})\, dy \\
&= -\int_{-y_0}^{y_0} \left(\frac{\partial^2 \mathbf{u}}{\partial y \partial t}\right)^T B\left(\frac{\partial \mathbf{u}}{\partial y} + \sigma \mathbf{w}\right) dy + \frac{\partial \mathbf{u}}{\partial t}^T B\left(\frac{\partial \mathbf{u}}{\partial y} + \sigma \mathbf{w}\right)\Big|_{-y_0}^{y_0}.
\end{aligned} \tag{45}$$

If we impose the transformed boundary condition (40), at $y = \pm y_0$ we obtain

$$\frac{\partial \mathbf{u}}{\partial t}^T B\left(\frac{\partial \mathbf{u}}{\partial y} + \sigma \mathbf{w}\right)\Big|_{-y_0}^{y_0} = 0.$$

For the transformed boundary condition (41), we have

$$\sigma \frac{\partial \mathbf{u}}{\partial t}^T \left(B\mathbf{w} + C^T \mathbf{v}\right)\Big|_{-y_0}^{y_0}.$$

Since both (40) and (41) hold, the boundary terms above also vanish. When all boundary terms vanish we have

$$\begin{aligned}
&\frac{1}{2}\frac{d}{dt}\int_{-y_0}^{y_0} \left(\Big|\frac{\partial \mathbf{u}}{\partial t}\Big|^2 + \frac{\partial \mathbf{u}}{\partial y} B \frac{\partial \mathbf{u}}{\partial y} + 2\frac{\partial \mathbf{u}}{\partial y}^T B\sigma \mathbf{w}\right) dy \\
&= \int_{-y_0}^{y_0} \left(\frac{\partial \mathbf{u}}{\partial y}^T B\sigma \frac{\partial \mathbf{w}}{\partial t} - \frac{\partial \mathbf{u}}{\partial t}^T \sigma \frac{\partial \mathbf{u}}{\partial t} + \frac{\partial \mathbf{u}}{\partial t}^T \sigma\alpha\,(\mathbf{u}-\mathbf{q})\right) dy.
\end{aligned} \tag{46}$$

By adding

$$\frac{d}{dt}\int_{-y_0}^{y_0} (\sigma \mathbf{w})^T B\,(\sigma \mathbf{w})\, dy, \quad \frac{1}{2}\frac{d}{dt}\int_{-y_0}^{y_0} \left(\sqrt{\alpha\sigma}\,(\mathbf{w}-\mathbf{q})\right)^T \left(\sqrt{\alpha\sigma}\,(\mathbf{u}-\mathbf{q})\right) dy,$$

to both sides of equation (46) we have

$$\begin{aligned}
\frac{1}{2}\frac{d}{dt}E_\sigma(t) = &\int_{-y_0}^{y_0} \left(\frac{\partial \mathbf{u}}{\partial y}^T B\sigma \frac{\partial \mathbf{w}}{\partial t} + 2\frac{\partial \mathbf{w}}{\partial t}^T B\sigma^2 \mathbf{w}\right) dy \\
&- \int_{-y_0}^{y_0} \left(\frac{\partial u}{\partial t}^T \sigma \frac{\partial u}{\partial t} - \frac{\partial \mathbf{u}}{\partial t}^T \sigma\alpha\,(\mathbf{u}-\mathbf{q}) - \frac{\partial\,(\mathbf{u}-\mathbf{q})}{\partial t}^T \sigma\alpha\,(\mathbf{u}-\mathbf{q})\right) dy.
\end{aligned} \tag{47}$$

On the LHS of (47) we recognize the energy (42). Using the auxiliary differential equations on the RHS of (47) we have

$$\begin{aligned}\frac{1}{2}\frac{d}{dt}E_\sigma =&\frac{d}{dt}\int_{-y_0}^{y_0}\left(\sigma\left(\frac{\partial \mathbf{u}}{\partial y}+\sigma\mathbf{w}\right)^T B\left(\frac{\partial \mathbf{u}}{\partial y}+\sigma\mathbf{w}\right)-\alpha\left(\frac{\partial \mathbf{u}}{\partial y}+\sigma\mathbf{w}\right)^T B\sigma\mathbf{w}\right)dy\\ &-\frac{d}{dt}\int_{-y_0}^{y_0}\left(\sigma\left(\alpha+\sigma\right)\mathbf{w}^T B\sigma\mathbf{w}+\frac{\partial\left(\mathbf{u}-\mathbf{q}\right)}{\partial t}^T\sigma\frac{\partial\left(\mathbf{u}-\mathbf{q}\right)}{\partial t}\right)dy.\end{aligned} \tag{48}$$

Thus Cauchy–Schwartz inequality yields

$$\frac{d}{dt}\sqrt{E_\sigma}\leq\left(\alpha_\infty+\sigma_\infty\right)\sqrt{E_\sigma}. \tag{49}$$

Gronwall's lemma yields the estimate

$$\sqrt{E_\sigma\left(t\right)}\leq e^{\beta t}\sqrt{E_\sigma\left(0\right)},\quad \beta=\alpha_\infty+\sigma_\infty.$$

□

If we can derive a discrete energy estimate analogous to (44), we say that the numerical approximation is strictly stable.

The corresponding semi–discrete SBP–SAT approximation is

$$\begin{aligned}&\frac{d^2\mathbf{u}}{dt^2}+\sigma\frac{d\mathbf{u}}{dt}=\left(\left(B\otimes D_2\right)-\tau\left(I_2\otimes H_y^{-1}\right)\left(I_2\otimes B_N\right)\left(B\otimes S\right)\right)\mathbf{u}+\mathbf{f}_b,\\ &\frac{d\mathbf{v}}{dt}=-\left(\sigma+\alpha\right)\mathbf{v},\\ &\frac{d\mathbf{w}}{dt}=-\alpha\mathbf{w}+\left(I_2\otimes D_1\right)\mathbf{u},\\ &\frac{d\mathbf{q}}{dt}=\alpha\left(\mathbf{u}-\mathbf{q}\right).\end{aligned} \tag{50}$$

As before, the forcing function $\mathbf{f}_b$ ensures perfect matching. Note also that $b=1$ corresponds to the transformed (40) and $b=2$ corresponds to (41). When $b=1$ we have

$$\mathbf{f}_1=\left(B\otimes D_1\right)\left(\sigma\mathbf{w}\right)+\sigma\alpha\left(\mathbf{u}-\mathbf{q}\right)-\tau\sigma\left(I_2\otimes H^{-1}\right)\left(I_2\otimes B_N\right)\left(B\otimes I\right)\mathbf{w}, \tag{51}$$

and $b=2$ yields

$$\mathbf{f}_2=\left(B\otimes D_1\right)\left(\sigma\mathbf{w}\right)+\sigma\alpha\left(\mathbf{u}-\mathbf{q}\right)+\tau\sigma\left(I_2\otimes H^{-1}\right)\left(I_2\otimes B_N\right)\left(C^T\otimes I\right)\mathbf{v}. \tag{52}$$

We will use (see [6])

$$M = D_1^T H D_1 + R, \quad R = R^T \geq 0.$$

To derive a corresponding discrete energy estimate, we introduce the relevant energy norm

$$\begin{aligned}\mathcal{E}_\sigma(t) = \frac{d\mathbf{u}}{dt}^T (I_2 \otimes H) \frac{d\mathbf{u}}{dt} + ((I_2 \otimes D_1)\mathbf{u} + \sigma\mathbf{w})^T (B \otimes H)((I_2 \otimes D_1)\mathbf{u} + \sigma\mathbf{w}) \\ + \mathbf{u}^T (B \otimes R)\mathbf{u} + (\sigma\mathbf{w})^T (B \otimes H)(\sigma\mathbf{w}) + \alpha\sigma(\mathbf{u} - \mathbf{q})^T (I_2 \otimes H)(\mathbf{u} - \mathbf{q}).\end{aligned} \tag{53}$$

Note that when $\sigma \equiv 0$ we get the standard physical energy for the semi–discrete wave equation

$$\mathcal{E}(t) = \frac{d\mathbf{u}}{dt}^T (I_2 \otimes H) \frac{d\mathbf{u}}{dt} + ((I_2 \otimes D_1)\mathbf{u})^T (B \otimes H)((I_2 \otimes D_1)\mathbf{u}) + \mathbf{u}^T (B \otimes R)\mathbf{u}. \tag{54}$$

We have

Proposition 4 *The 1D semi-discrete perfectly matched layer (50) subject to the transformed boundary condition (40) at $y = \pm y_0$, satisfies*

$$\sqrt{\mathcal{E}_\sigma(t)} \leq e^{\beta t}\sqrt{\mathcal{E}_\sigma(0)}, \quad \beta = \alpha_\infty + \sigma_\infty. \tag{55}$$

Proof:

To derive the estimate (55), we multiply (50) by $(d\mathbf{u}/dt)^T (I_2 \otimes H)$, having

$$\begin{aligned}\frac{1}{2}\frac{d}{dt}\tilde{\mathcal{E}} = \sigma((I_2 \otimes D_1)\mathbf{u})^T (B \otimes H)\frac{d\mathbf{w}}{dt} - \sigma\frac{d\mathbf{u}}{dt}^T (I_2 \otimes H)\frac{d\mathbf{u}}{dt} + \sigma\alpha\frac{d\mathbf{u}}{dt}^T (I_2 \otimes H)(\mathbf{u} - \mathbf{q}) \\ + (1 - \tau)\frac{d\mathbf{u}}{dt}^T (B \otimes H)((I_2 \otimes B_N S)\mathbf{u} + \sigma(I_2 \otimes B_N)\mathbf{w}),\end{aligned} \tag{56}$$

where

$$\begin{aligned}\tilde{\mathcal{E}} = \frac{d\mathbf{u}}{dt}^T (I_2 \otimes H)\frac{d\mathbf{u}}{dt} + ((I_2 \otimes D_1)\mathbf{u})^T (B \otimes H)(I_2 \otimes D_1)\mathbf{u} \\ + 2\sigma((I_2 \otimes D_1)\mathbf{u})^T (B \otimes H)\mathbf{w} + \mathbf{u}^T((B \otimes R))\mathbf{u}.\end{aligned}$$

The last term in (56) is a boundary term. Consider now the transformed boundary condition (40), (with $\tau = 1$) we have

$$(1 - \tau)\frac{d\mathbf{u}}{dt}^T (B \otimes H)((I_2 \otimes B_N S)\mathbf{u} + \sigma(I_2 \otimes B_N)\mathbf{w}) \equiv 0.$$

When the boundary terms vanish we have

$$\frac{1}{2}\frac{d}{dt}\tilde{\mathcal{E}} = \sigma\left(\left(I_2 \otimes D_1\right)\mathbf{u}\right)^T\left(B \otimes H\right)\frac{d\mathbf{w}}{dt} - \sigma\frac{d\mathbf{u}}{dt}^T\left(I_2 \otimes H\right)\frac{d\mathbf{u}}{dt} + \sigma\alpha\frac{d\mathbf{u}}{dt}^T\left(I_2 \otimes H\right)\left(\mathbf{u}-\mathbf{q}\right). \tag{57}$$

By adding

$$\frac{d}{dt}\left(\left(\sigma\mathbf{w}\right)^T\left(B \otimes H\right)\left(\sigma\mathbf{w}\right)\right), \quad \frac{1}{2}\alpha\sigma\frac{d}{dt}\left(\left(\mathbf{u}-\mathbf{q}\right)^T\left(I_2 \otimes H\right)\left(\mathbf{u}-\mathbf{q}\right)\right),$$

to both sides of equation (57) we have

$$\begin{aligned}\frac{1}{2}\frac{d}{dt}\mathcal{E}_\sigma = {} & \sigma\left(\left(I_2 \otimes D_1\right)\mathbf{u}\right)^T\left(B \otimes H\right)\frac{d\mathbf{w}}{dt} - \sigma\frac{d\mathbf{u}}{dt}^T\left(I_2 \otimes H\right)\frac{d\mathbf{u}}{dt} + \sigma\alpha\frac{d\mathbf{u}}{dt}^T\left(I_2 \otimes H\right)\left(\mathbf{u}-\mathbf{q}\right) \\ & 2\left(\frac{d}{dt}\sigma\mathbf{w}\right)^T\left(B \otimes H\right)\left(\sigma\mathbf{w}\right) + \frac{1}{2}\alpha\sigma\left(\frac{d}{dt}\left(\mathbf{u}-\mathbf{q}\right)\right)^T\left(I_2 \otimes H\right)\left(\mathbf{u}-\mathbf{q}\right).\end{aligned} \tag{58}$$

By using the discrete auxiliary differential equation on the RHS of (58) we have

$$\begin{aligned}\frac{1}{2}\frac{d}{dt}\mathcal{E}_\sigma = {} & \sigma\left(\left(I_2 \otimes D_1\right)\mathbf{u} + \sigma\mathbf{w}\right)^T\left(B \otimes H\right)\left(\left(I_2 \otimes D_1\right)\mathbf{u} + \sigma\mathbf{w}\right) \\ & - \alpha\left(\left(I_2 \otimes D_1\right)\mathbf{u} + \sigma\mathbf{w}\right)^T\left(B \otimes H\right)\sigma\mathbf{w} - \sigma\left(\alpha+\sigma\right)\mathbf{w}^T\left(B \otimes H\right)\sigma\mathbf{w} \\ & - \left(\frac{d\left(\mathbf{u}-\mathbf{q}\right)}{dt}\right)^T\left(I_2 \otimes H\right)\sigma\frac{d\left(\mathbf{u}-\mathbf{q}\right)}{dt}.\end{aligned} \tag{59}$$

Cauchy–Schwartz inequality yields

$$\frac{d}{dt}\sqrt{\mathcal{E}_\sigma} \leq \left(\alpha_\infty + \sigma_\infty\right)\sqrt{\mathcal{E}_\sigma}. \tag{60}$$

Gronwall's lemma yields the estimate

$$\sqrt{\mathcal{E}_\sigma\left(t\right)} \leq e^{\beta t}\sqrt{\mathcal{E}_\sigma\left(0\right)}, \quad \beta = \alpha_\infty + \sigma_\infty.$$

□

Remark 1 *When we impose the boundary condition (41), there is a non vanishing boundary term*

$$\sigma\left(\frac{d\mathbf{u}}{dt}^T\left(B \otimes B_N\right)\mathbf{w} + \frac{d\mathbf{u}}{dt}^T\left(C^T \otimes B_N\right)\mathbf{v}\right) \neq 0.$$

Because of this remaining boundary term, for the transformed boundary condition (41), we are unable to estimate the solutions in the energy norm. As we will see below and from the numerical experiments in the next section, this can hamper the stability and the accuracy of our schemes.

5.3.2 2D problem and discrete eigenvalues

For the corresponding 2D PML, because of the mixed spatial derivatives, we could not derive both continuous and discrete energy estimates. We will instead compute the temporal eigenvalues of the fully discrete spatial operators at constant coefficients. Consider the semi–discrete PML (33), (35) with second order accurate SBP operators and 2π–periodicity in the x–direction. The waveguide is normalized such that $-1 \leq y \leq 1$. Note that

$$\Delta x = 2\pi/N_x, \quad \Delta y = 2/N_y,$$

where $N_x = 2m$ such that $m\Delta x = \pi$. The grid functions are 2π–periodic functions in the x–direction, $\mathbf{u}_{ij} = \mathbf{u}_{ij+N_x}$. As before, we take discrete Fourier transform in the x–direction. The corresponding eigenvalue problem is

$$\left(\mathcal{P}_b - \lambda \mathbf{I}\right) \mathbf{U} = 0, \quad b = 1, 2, \quad \mathbf{U} = \left(\mathbf{u}, \mathbf{u}_t, \mathbf{v}, \mathbf{w}, \mathbf{q}\right)^T, \tag{61}$$

where $\mathcal{P}_b$ is the fully discrete spatial operator including the transformed boundary condition (17) with $b = 1$ and (18) with $b = 2$. For the transformed boundary condition (17) the corresponding spatial operator is

$$\mathcal{P}_1 = \begin{pmatrix} \mathbf{0} \otimes \mathbf{I} & \mathbf{I}_2 \otimes \mathbf{I} & \mathbf{0} \otimes \mathbf{I} & \mathbf{0} \otimes \mathbf{I} & \mathbf{0} \otimes \mathbf{I} \\ \mathbf{L} + \alpha\sigma \left(\mathbf{I}_2 \otimes \mathbf{I}\right) & -\sigma \left(\mathbf{I}_2 \otimes \mathbf{I}\right) & -i\frac{\sin(\Delta x k_x)}{\Delta x}\sigma A \otimes \mathbf{I} & \sigma B \otimes \left(D_1 - \tau B_N\right) & -\alpha\sigma \left(\mathbf{I}_2 \otimes \mathbf{I}\right) \\ i\frac{\sin(\Delta x k_x)}{\Delta x}\mathbf{I}_2 \otimes \mathbf{I} & \mathbf{0} \otimes \mathbf{I} & -\left(\alpha + \sigma\right)\mathbf{I}_2 \otimes \mathbf{I} & \mathbf{0} \otimes \mathbf{I} & \mathbf{0} \otimes \mathbf{I} \\ \mathbf{I}_2 \otimes D_1 & \mathbf{0} \otimes \mathbf{I} & \mathbf{0} \otimes \mathbf{I} & -\alpha \mathbf{I}_2 \otimes \mathbf{I} & \mathbf{0} \otimes \mathbf{I} \\ \alpha \mathbf{I}_2 \otimes \mathbf{I} & \mathbf{0} \otimes \mathbf{I} & \mathbf{0} \otimes \mathbf{I} & \mathbf{0} \otimes \mathbf{I} & -\alpha \mathbf{I}_2 \otimes \mathbf{I} \end{pmatrix},$$

and for the transformed boundary condition (18) we have

$$\mathcal{P}_2 = \begin{pmatrix} \mathbf{0} \otimes \mathbf{I} & \mathbf{I}_2 \otimes \mathbf{I} & \mathbf{0} \otimes \mathbf{I} & \mathbf{0} \otimes \mathbf{I} & \mathbf{0} \otimes \\ \mathbf{L} + \eta\sigma \left(\mathbf{I}_2 \otimes \mathbf{I}\right) & -\sigma \left(\mathbf{I}_2 \otimes \mathbf{I}\right) & -i\frac{\sin(\Delta x k_x)}{\Delta x}\sigma A \otimes \mathbf{I} + \tau\sigma \left(C^T \otimes B_N\right) & \sigma B \otimes \left(D_1\right) & -\alpha\sigma \left(\mathbf{I} \\ i\frac{\sin(\Delta x k_x)}{\Delta x}\mathbf{I}_2 \otimes \mathbf{I} & \mathbf{0} \otimes \mathbf{I} & -\left(\alpha + \sigma\right)\mathbf{I}_2 \otimes \mathbf{I} & \mathbf{0} \otimes \mathbf{I} & \mathbf{0} \otimes \\ \mathbf{I}_2 \otimes D_1 & \mathbf{0} \otimes \mathbf{I} & \mathbf{0} \otimes \mathbf{I} & -\alpha \mathbf{I}_2 \otimes \mathbf{I} & \mathbf{0} \otimes \\ \alpha \mathbf{I}_2 \otimes \mathbf{I} & \mathbf{0} \otimes \mathbf{I} & \mathbf{0} \otimes \mathbf{I} & \mathbf{0} \otimes \mathbf{I} & -\alpha \mathbf{I}_2 \end{pmatrix}$$

Here

$$\begin{aligned} \mathbf{L} = & -4\frac{\sin^2\left(\Delta x k_x/2\right)}{\Delta x^2} A \otimes \mathbf{I} + i\frac{\sin\left(\Delta x k_x\right)}{\Delta x}\left(C + C^T\right) \otimes D_1 + B \otimes D_2 \\ & - \tau \left(H^{-1} B_N \otimes I_2\right) \left(B \otimes D_1 + i\frac{\sin\left(\Delta x k_x\right)}{\Delta x} C^T \otimes I\right), \end{aligned}$$

is the discrete spatial operator for the elastic wave equation (2) with a SAT imposition of the free–surface boundary condition (4).

Note that only discrete wave numbers

$$k_x \in \{-m, -m+1, \ldots, -1, 0, 1, \ldots, m-1, m\},$$

can be represented, unlike a continuous problem where k_x takes any real value. It is important to see that no nonzero wavenumber $|k_x| < 1$ can be present. For the aluminum waveguide with $\gamma = 0.4593$ all backward propagating modes correspond to nonzero wavenumber with $|k_x| < 1$. The discrete approximation excludes all backward propagating modes for a 2π–periodic PML in an aluminum waveguide. Thus we must expect all eigenvalues of $\mathcal{P}_b$ to have non–positive real parts.

Note that in real applications only a few grid points are used in the PML. Therefore, the PML width is always short, and only modes with short wavelengths can be supported in the PML. In [15], for computational domains completely surrounded by the PML, we determined the number of grid points needed for a stable discrete PML, for various anisotropic elastic materials violating the geometric stability condition.

As before, we set $\sigma = 1, \alpha = 0.1$. Consider the aluminum waveguide defined by the velocity ratio $\gamma = 0.4593$. To compute the eigenvalues of the operator $\mathcal{P}_b$ we use $N_x + 1 = N_y + 1 = 101$ grid points in both x– and y–directions.

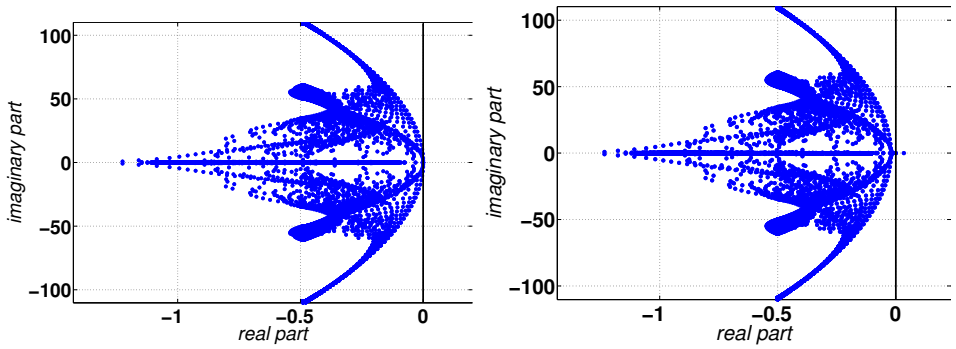

Figure 3: *Temporal eigenvalues of the fully discrete spatial operator. In the figure to the left, the boundary condition is (17) at $y = \pm 1$ and to the right, the boundary conditions is (18) at $y = \pm 1$. The damping coefficient is $\sigma = 1$ and the complex frequency shift is $\alpha = 0.1$. Note that (to the right) for the boundary conditions (18) there are purely real positive eigenvalues.*

In figure 3, we have plotted the eigenvalues of of the operators $\mathcal{P}_1$ and $\mathcal{P}_2$. Note that for the operator $\mathcal{P}_1$ all eigenvalues have non–positive real parts. We conclude that the transformed boundary condition (17) yields numerically stable solutions.

On the other hand, the operator $\mathcal{P}_2$ has eigenvalues with positive real parts. All eigenvalues with positive real parts are purely real. Note that when

$\sigma \equiv 0$ there are multiple zero eigenvalues. When $\sigma > 0$ some of the these multiple zero eigenvalues move into the right half of the complex plane. We conclude that the transformed boundary condition (18) leads to temporally growing solutions. Note also that the positive eigenvalues correspond to lower spatial wavenumbers (see also figure 2), close to where backward propagating modes could possibly exist. This instability could mistakenly be attributed to backward propagating modes, and not to the ill–treatment (or wrong formulation) of the discrete boundary conditions.

The analysis here will present themselves more in the next section when numerical simulations are presented.

5.4 Fully discrete approximation

We introduce the discrete time variable, $t_n = n\triangle t$, $n \in \mathbb{N}$, $\triangle t$ is the time step and $u^n \approx u(t_n)$. The usual finite difference operators (with respect to time) and the shift operator are denoted

$$\begin{aligned} \triangle t^2 D^{tt}\mathbf{u}^n &= \mathbf{u}^{n+1} - 2\mathbf{u}^n + \mathbf{u}^{n-1}, \quad 2\triangle t D_0^t \mathbf{u}^n = \mathbf{u}^{n+1} - \mathbf{u}^{n-1}, \\ \triangle t D_+^t \mathbf{u}^n &= \mathbf{u}^{n+1} - \mathbf{u}^n, \quad S^t \mathbf{u}^n = \mathbf{u}^{n+1}. \end{aligned}$$

The time integration uses the compact time-stepping scheme [17], for the physical variable $\mathbf{u}$, and the Crank-Nicolson scheme for the auxiliary variables $\mathbf{v}, \mathbf{w}, \mathbf{q}$. A second order accurate time-stepping scheme is

$$\begin{aligned} D^{tt}\mathbf{u}^n + \sigma D_0^t \mathbf{u}^n &= L\mathbf{u}^n + F_b^n \\ D_+^t \mathbf{v}^n &= \frac{1}{2}(I + S^t)((I_2 \otimes D_x)\,\mathbf{u}^n - (\sigma + \alpha)\,\mathbf{v}^n), \\ D_+^t \mathbf{w}^n &= \frac{1}{2}(I + S^t)\left((I_2 \otimes D_y)\,\mathbf{u}^n - \alpha \mathbf{w}^n\right), \\ D_+^t \mathbf{q}^n &= \alpha\frac{1}{2}(I + S^t)\left(\mathbf{u}^n - \mathbf{q}^n\right). \end{aligned} \tag{62}$$

6 Numerical experiments

In this section, we present numerical experiments. The experiments aim at verifying the above analyses. As an example we will consider a rectangular aluminum waveguide (with the velocity ratio $\gamma = 0.4593$), bounded in the y-direction by free-surface boundary conditions. The frequency domain PML for this material has been studied in [10]. We will begin by investigating the stability of the discrete PML for the transformed boundary conditions (17), (18) and the physical boundary condition (4). Lastly, we will make a convergence study.

6.1 Stability

In the first set of experiments, we investigate numerically the stability of the PML in an elastic waveguide subject to the free–surface boundary conditions. We consider the rectangular computational domain $(x, y) \in [-1, 1] \times [-1, 1]$ with the PML everywhere. The damping is $\sigma = 2$ and the complex frequency shift is $\alpha = 0.1$. We are particularly interested in the temporal behavior of the numerical solutions when we impose the transformed boundary conditions (17), (18) or the physical boundary condition (4), in the PML.

Consider the initial data

$$u(x, y, 0) = v(x, y, 0) = \sin \pi x \cos 2\pi y, \tag{63}$$

for the displacement fields. We set homogeneous initial data for the velocity fields and all auxiliary variables. A uniform spatial step $\Delta x = \Delta y = 0.02$ is used in both x– and y– directions. The boundary conditions at $y = \pm 1$ is the transformed boundary conditions (17), (18) or the physical boundary condition (4). Homogeneous Dirichlet boundary condition on the displacement field is set at $x = \pm 1$. The time–step is $dt = 0.2\Delta x$. We run the simulation until $t = 200$ (50, 000 time–steps) and record the elastic energy in the L_2 norm. Numerical results are shown in figure 4.

Note that the transformed boundary condition (17) yields a numerically stable scheme. For (17) all solutions remain bounded even at late times. The numerical solutions corresponding to the transformed boundary condition (18) grow linearly. This is not a desirable property if long time simulations are required. When we use the physical boundary condition (4), without any modification, the numerical solutions grow exponentially in time.

6.2 Accuracy

To investigate accuracy, we consider an infinitely long rectangular aluminum waveguide (with $\gamma = 0.4593$), bounded in the y–direction by free–surface boundary conditions. We truncate the waveguide in the x–direction and normalize such that the truncated domain has dimensions $(x, y) \in [-1, 1] \times [-1, 1]$. We surround the artificial boundaries with PML of width $\delta = 0.2$ having $(x, y) \in [-1 - \delta, 1 + \delta] \times [-1, 1]$. We discretize the domain with a uniform spatial step $\Delta x = \Delta y = h$ in both x– and y–directions. The time–step is $dt = 0.2h$. In this experiments the aim is to study the accuracy of the layer.

Note that when a PML model is used in a numerical computation, errors can be divided into three different categories: the discretization error, numerical reflection, and the modeling error. The discretization error is the

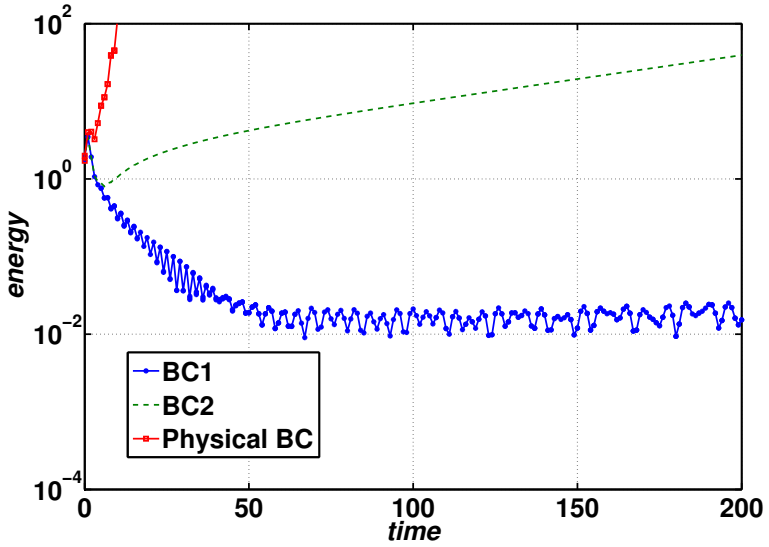

Figure 4: *Time history of L_2 norm of the elastic energy $\left\|\sqrt{u^2+v^2}\right\|$ with various boundary conditions in the PML. The curve BC1 corresponds to using the transformed boundary condition (17), the curve BC2 corresponds to using the transformed boundary condition (18) and the curve Physical BC corresponds to using the free–surface boundary condition (4) without modification.*

generic error that comes with any numerical method (for example by approximating derivatives by differences). The numerical reflections are the spurious discrete effects introduced by discretizing the PML and seen in the interior domain. The modeling error is introduced because the layer has a finite width. The discretization error and numerical reflection should vanish as the mesh-size approaches zero and the modeling error decreases as the magnitude of damping coefficient or the PML width increases.

We can choose the PML parameters (for a fixed PML width) as a function of the grid-size h such that the total PML error (modeling error + numerical reflection) converges to zero at the rate $O(h^p|\log(h)|)$. Here, $p = 2, 4$ is the order of accuracy of the interior scheme.

In the following experiments we consider the homogeneous initial data

$$\mathbf{u}(x,y,0) = \frac{\partial}{\partial t}\mathbf{u}(x,y,0) = \mathbf{v}(x,y,0) = \mathbf{w}(x,y,0) = \mathbf{q}(x,y,0) = 0, \qquad (64)$$

for all field variables (both the physical and the auxiliary variables). We force the first component of the displacement field with the Ricker Wavelet

trucanted by a Gaussian

$$f(x,y,t) = h(t)\, e^{-\left(x^2+(y-0.8)^2\right)/\delta^2}, \quad \delta = 0.05,$$
$$h(t) = (2\pi f_0)^2 \left((4\pi (f_0 t - 1))^2 - 1 \right) e^{-2\pi (f_0 t - 1)^2}, \quad f_0 = 10.$$

The damping profile is the quadratic monomial,

$$\sigma(x) = \begin{cases} 0 & \text{if} \quad |x| \le 1, \\ d_0 \left(\frac{|x|-1}{\delta} \right)^2 & \text{if} \quad |x| \ge 1, \end{cases} \quad d_0 > 0,$$

where the PML width is $\delta = 0.2$. We set $d_0 = 3/(2 \times \delta)\, c_p \log(1/(C_0 h)^p)$ so that numerical reflection from the interface will be small compared to to the modeling error. We have used a second order ($p = 2$) and a fourth order ($p = 4$) accurate schemes respectively, in the interior. The parameter $c_p = 2.2$ is the maximum wave speed and $C_0 = 0.1$ is empirically determined. In this case the numerical scheme in the interior converges at the rate $O(h^p)$. Therefore the discretization error converges at the rate $O(h^p)$, the modeling error converges at the rate $\exp(-\int \sigma d\xi) = O(h^p)$ and the numerical reflection converges at the rate $O(d_0 h^p) = O(h^p |\log(h)|)$. At best, the total PML error is expected to approach zero at the rate $O(h^p |\log(h)|)$.

To begin with, we compute the solutions using the 4th order accurate scheme, with the mesh–size $h = 0.01$. The complex frequency shift is $\alpha = 0.1$. In figure 5, we display the snapshots of the solutions at different times. Note that all waves propagating into the PML are absorbed without reflections. Waves propagating to the walls of the waveguide at $y = \pm 1$ are reflected.

In order to measure errors, a reference solution is computed in a larger domain $(x, y) \in [-5, 5] \times [-1, 1]$ without the PML. By comparing the solutions in the interior to the reference solution in the L_2–norm we obtain an accurate measure of numerical errors. We have used a second and a fourth order accurate schemes in the interior, for two different cases. The two boundary conditions (17) and (18) are considered separately. In figure 6 and table 1 we display numerical errors for the transformed boundary condition (17) with different resolutions. The corresponding numerical errors for the transformed boundary condition (18) are displayed in figure 7 and table 2.

Apparently, the PML with the transformed boundary condition (17) yields high order convergence rate of PML errors. On the other hand, the transformed boundary condition (18) leads to a loss of accuracy in the PML. In this case the second order scheme yields first order accuracy and the fourth order scheme yields a convergence rate less than third order accuracy. Note

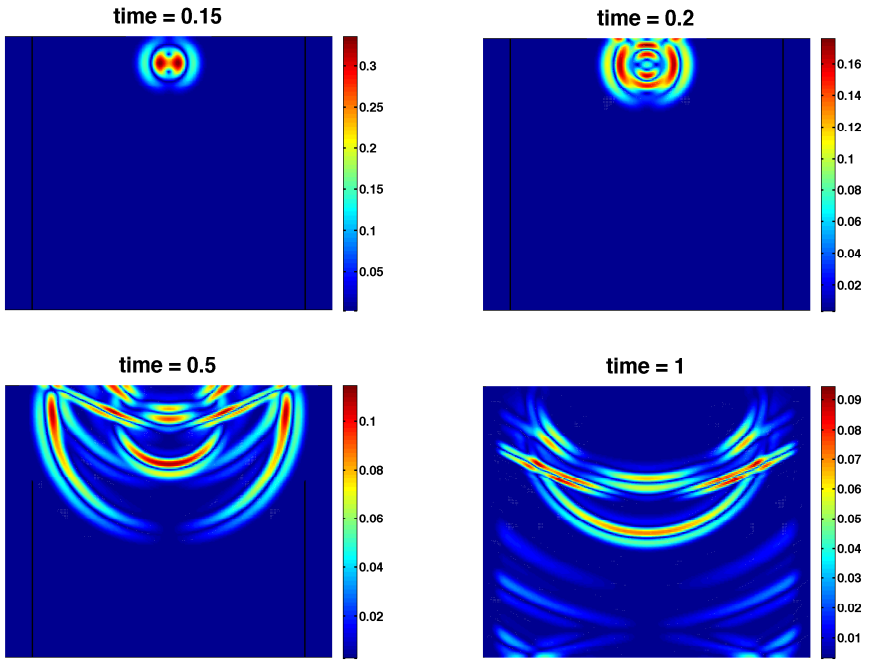

Figure 5: *The dynamics of the elastic energy* $\sqrt{u_1^2 + u_2^2}$ *inside an elastic waveguide bounded by traction-free boundary conditions at* $y = \pm 1$*, the waveguide is truncated at* $x = \pm 1$ *with the PML of width* $\delta = 0.2$*. The boundary conditions at* $x = \pm 1.2$ *are homogeneous Dirichlet boundary conditions for the displacement fields. The snapshots are give at* $t = 0.15, 0.2, 0.5, 1.0$*.*

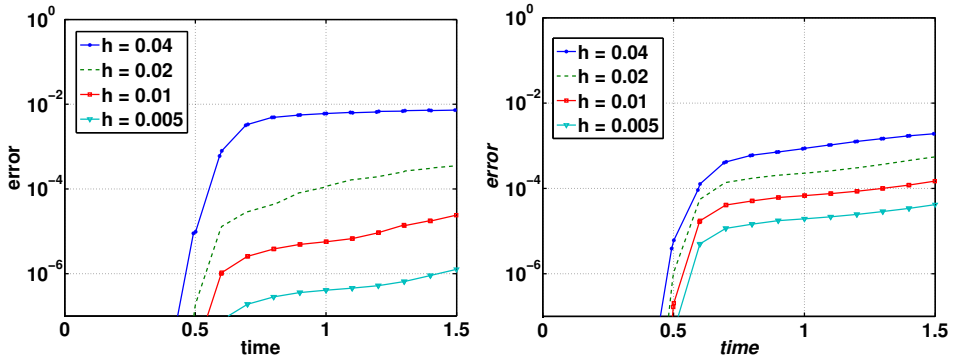

Figure 6: *Total PML error as a function of grid-size* h*, for the CFS–PML with* $B\mathbf{u}_y(x, \pm 1, t) + C^T \mathbf{u}_x(x, \pm 1, t) + \sigma B \mathbf{w}(x, \pm 1, t) = 0$*.*

that similar results were obtain in [18] for the scalar wave equation with homogeneous Neumann conditions on the walls of the waveguide.

Mesh-size	4–th Order		2–nd Order	
(h)	**error**	**rate**	**error**	**rate**
0.04	7.3000×10^{-3}	–	1.9000×10^{-3}	–
0.02	3.5203×10^{-4}	4.3687	5.4807×10^{-4}	1.8012
0.01	2.4071×10^{-5}	3.8703	1.4816×10^{-4}	1.8873
0.005	1.2665×10^{-6}	4.2485	4.1699×10^{-5}	1.8290

Table 1: *Total PML error as a function of grid-size h, for the CFS–PML with* $B\mathbf{u}_y(x,\pm1,t) + C^T\mathbf{u}_x(x,\pm1,t) + \sigma B\mathbf{w}(x,\pm1,t) = 0$.

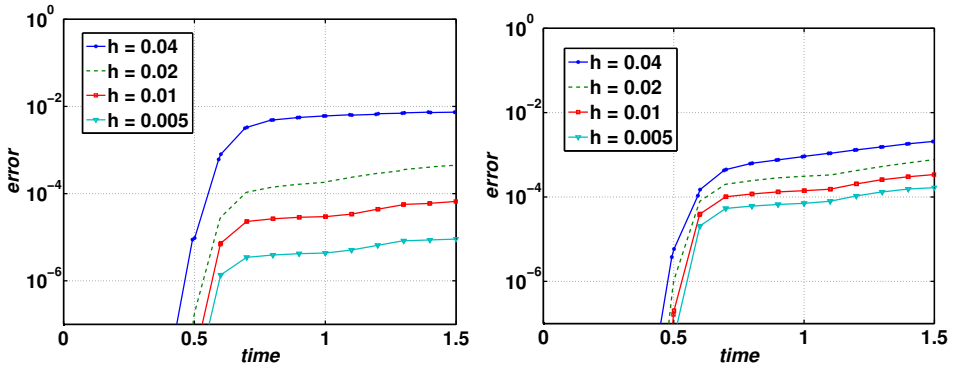

Figure 7: *Total PML error as a function of grid-size h, for the CFS–PML with* $B\mathbf{u}_y(x,\pm1,t) + C^T\mathbf{u}_x(x,\pm1,t) - \sigma C^T\mathbf{v}(x,\pm1,t) = 0$.

Mesh-size	4–th Order		2–nd Order	
(h)	**error**	**rate**	**error**	**rate**
0.04	7.4000×10^{-3}	–	2.1000×10^{-3}	–
0.02	4.4882×10^{-4}	4.0430	7.6791×10^{-4}	1.4303
0.01	6.6171×10^{-5}	2.7618	3.3925×10^{-4}	1.1786
0.005	9.0577×10^{-6}	2.8690	1.6642×10^{-4}	1.0275

Table 2: *Total PML error as a function of grid-size h, for the CFS–PML with* $B\mathbf{u}_y(x,\pm1,t) + C^T\mathbf{u}_x(x,\pm1,t) - \sigma C^T\mathbf{v}(x,\pm1,t) = 0$.

7 Conclusions

This paper concludes our work on the accuracy and the stability of the PML for second order time-dependent wave equations when physical boundary conditions are important. We have demonstrated in both theory and numerical experiments that the PML remains a potential tool to simulate the absorptions of waves in numerical wave simulators. A main result is that if the underlying boundary conditions involve normal derivatives (normal with the PML), the boundary conditions must be transformed using the PML metric. Secondly, in the discrete setting the formulation of the bound-

ary conditions (the choice of auxiliary variables) is crucial in order to ensure stable and accurate discrete PML.

References

[1] N. A. Petersson, B. Sjögreen, *An energy absorbing far-field boundary condition for the ElasticWave Equation*, Commun. Comput. Phys., 6, p 483–508, (2009).

[2] B. Sjögreen, N. A. Petersson, *Perfectly matched layer for Maxwell's equation in second order formulation*, J Comp Phys, 209, p19–46, 2005.

[3] M. H. Carpenter, D. Gottlieb, S. Abarbanel, *Time-stable boundary conditions for finite-difference schemes solving hyperbolic systems: methodology and application to high-order compact schemes*, J. of Comp. Phys, 111(2), p 220-236 (1994).

[4] K. Mattsson, F. Ham, G. Iaccarino, *Stable boundary treatment for the wave equation on second order form*, J Comp Phys, 227, p8753–8767, (2008).

[5] M. Svärd , J. Nordström, *On the order of accuracy for difference approximations of initial-boundary value problems*, J Comp Phys, 218, p333–352, (2006).

[6] K. Mattsson, F. Ham, G. Iaccarino, *Stable boundary treatment for the wave equation in second-order form*, J Sci Comput, 41, p336–383, (2009).

[7] B. Gustafsson, *High order difference methods for time dependent PDE*, Springer–Verlag, Berlin Heidelberg, 2008.

[8] H-O Kreiss, O E. Ortiz and N. A. Petersson, *Initial-boundary value problems for second order systems of partial differential equations*, Math Mod and Num Analys. Commun, (2009).

[9] E. Bécache, S. Fauqueux, P. Joly, *Stability of Perfectly Matched Layers, Group Velocities and Anisotropic Waves*, J. Comp. Phys., 188,p399-433, (2003).

[10] E. A. Skelton, S.D.M. Adams and R. V. Craster, *Guided elastic waves and perfectly matched layers,* Wave Motion, 44, p573–592, (2007).

[11] J. A Postnova, *Trapped modes in non-uniform elastic waveguides: asymptotic and numerical methods,* PhD Thesis. Imperial College London, (2009).

[12] M. Kuzuoglu and R. Mittra. Frequency Dependence of the Constitutive Parameters of Causal Perfectly Matched Anisotropic Absorbers. *IEEE Microwave and Guided Wave Letters,* 6, (1996).

[13] W. Chew and W. Weedon. A 3-D Perfectly Matched Medium from Modified Maxwell's Equations with Stretched Coordinates. *Micro. Opt. Tech. Lett.,* 7:599–604, (1994).

[14] K. Duru, G. Kreiss, *A Well–posed and discretely stable perfectly matched layer for elastic wave equations in second order formulation*, Commun. Comput. Phys., 11, 1643–1672, (2012).

[15] G. Kreiss, K. Duru, *Discrete stability of perfectly matched layers for anisotropic wave equations in first and second order formulation*, submitted to SIAM JSC (2011)

[16] K. Duru, *Perfectly matched layer for second order wave equations*, Licentiate Thesis, Div Sc. Comp., Dept. of Infor Tech., Uppsala University, ISSN 1404-5117; 2010–004, (2010).

[17] K. Duru, K. Mattsson, G. Kreiss, *Stable and conservative time propagators for second order hyperbolic systems*, Tech Rep, Div Sc. Comp., Dept. of Infor Tech., Uppsala University, 201–008, (2011).

[18] K. Duru, G. Kreiss, *On the accuracy and stability of the perfectly matched layers in transient waveguides*, J. of Sc. Comput., In press DOI: 10.1007/s10915-012-9594-7 (2012).

[19] K. Duru, G. Kreiss, K. Mattsson, *Accurate and stable boundary treatments for elastic wave equations in second formulation*, submitted to JCP, (2012).

[20] K. Duru, G. Kreiss, *Boundary waves and the stability of the perfectly matched layer*, to appear, (2012).

[21] J–P. Bérenger, *Numerical reflection from FDTD-PMLs: A comparison of the split PML with the unsplit and CFS PMLs,* IEEE transactions on antennas and propagation, Vol. 50, no. 3, (2003).

[22] M. J. Grote and Imbo Sim, *Efficient PML for the wave equation,* Dept. of Maths, University of Basel, Switzerland, (2009).

[23] B. Alpert, L. Greengard, T. Hagstrom. *Nonreflecting Boundary Conditions for the Time-Dependent Wave Equation,* J. of Comput. Phys 180, 270–296 (2002).

[24] F. Collino. High order absorbing boundary conditions for wave propagation models. Straight line and corner cases. *in: R. Kleinman, eta.*

(Eds.), Proceedings of the second international conference on mathematical and numerical aspects of waves, SIAM, Delaware, 161–171, (1993).

[25] B. Engquist and A. Majda. Absorbing boundary conditions for numerical simulation of waves. *Proc. Natl. Acad. Sci. USA,* 74:1765–1766, (1977).

[26] D. Givoli. High-order local non-reflecting boundary contions: a review. *Wave Motion* 39:319–326, (2004).

[27] M. Grote and I. Sim. *On local nonreflecting boundary conditions for time dependent wave propagation problems.* Dept. of Maths, University of Basel, Switzerland, (2009).

[28] T. Hagstrom, T. Warburton, D. Givoli. Radiation boundary boundary conditions for time-dpendent waves based on complete plane waves expansions. *J. Comput. Appl. Math.,* to appear.

[29] T. Rylander and J-M, Jin. Perfectly matched layer in three dimensions for the time-domain finite element method applied to radiation problems *IEEE Transact on Ant and Propagat*, Vol. 53, No 4 (2005).

[30] E. Abenius, F, Edelvik and C. Johansson. Waveguide truncation using UPML in the finite-element time-domain method

[31] E. Bécache, P. G. Petropoulos, and S. D. Gedney. On the Long-Time Behaviour of Unplit Perfectly Matched Layers. *IEEE Transactions on Antennas and Propagation,* 52, (2004).

[32] E. Bécache and P. Joly. On the analysis of Bérenger's perfectly matched layers for Maxwell's equations. *Math. Mod. and Num. Analys.,* 36:87–119, (2002).

[33] J–P. Bérenger, *Perfectly Matched Layer (PML) for Computational Electromagnetics*, Synthesis lectures on computational electromagnetics, Morgan and Claypool (2007).

[34] D. Appelö and T. Colonius, *A high order super-grid-scale absorbing layer and its application to linear hyperbolic systems*, J. Comp. Phys., 228 (11), 4200-4217, (2009).

[35] D. Appelö and G. Kreiss, *Application of a perfectly matched layer to the nonlinear wave equation*, Wave Motion Vol. 44, pp531-548 (2007)

[36] Y. Y. Lu and J. Zhu, D. *Propagating modes in optical waveguides terminated by perfectly matched layers*, IEEE Photonics Technology Letters, Vol. 17, No. 12, (2005)

[37] J–P. Bérenger, *Application of the CFS PML to the absorption of evanescent waves in waveguides*, IEEE Microwave and Wireless Components Letters, Vol. 12, No. 6, (2002).

[38] J–P. Bérenger, *A perfectly matched layer for the absorption of electromagnetic waves,* J. Comp. Phys., 114, 185–200, (1994).

[39] J. D. Achenbach, *Wave propagation in elastic solids*, volume 16 of Applied Mathematics and Mechanics. North–Holland, (1973)

[40] Lord Rayleigh, *On waves propagated along the plane surface of an elastic solid*, Proc. Lond. Math. Soc., 17 , pp. 4–11 (1885)

[41] H. Lamb, *On waves in an elastic plate*, Proc. R. Soc. Lond. A 93, 114-128 (1917)